JOURNAL OF GEOPHYSICAL RESEARCH, VOL. 113, D23209, doi:10.1029/2008JD009956, 2008

Chemical composition and morphology of individual aerosol particles from a CARIBIC flight at 10 km altitude between 50°N and 30°S

H. N. Nguyen,[1] B. G. Martinsson,[1] J. B. Wagner,[2,3] E. Carlemalm,[4] M. Ebert,[5] S. Weinbruch,[5] C. A. M. Brenninkmeijer,[6] J. Heintzenberg,[7] M. Hermann,[7] T. Schuck,[6] P. F. J. van Velthoven,[8] and A. Zahn[9]

Received 12 February 2008; revised 12 August 2008; accepted 28 August 2008; published 10 December 2008.

[1] Analysis of individual particles by analytical electron microscopy as well as quantitative analysis using particle-induced X-ray emission (PIXE) and particle elastic scattering analysis (PESA) were carried out on samples collected from a flight at 10 km altitude between 50°N and 30°S as part of the Civil Aircraft for Regular Investigation of the atmosphere Based on an Instrument Container (CARIBIC) project (http://www.caribic-atmospheric.com). Particle morphology showed large variability with sampling latitude. Complicated branched structures dominated the large particles of the extratropical northern and southern hemisphere and the northern tropics. Particles in the tropics of the southern hemisphere were small in size and large in number concentration, whereas particles in or close to the intertropical convergence zone were few and small in size. Particles in the lowermost stratosphere were found to have similar structures but more branched than the ones found in the upper troposphere of the extratropics. Quantitative analysis revealed that the sulfur concentration varied by a factor of 50 in the nine samples analyzed in this study. The carbon-to-sulfur mass concentration ratio was lowest in the lowermost stratosphere (0.5) and highest in the tropics of the southern hemisphere (3.5). The elemental distribution of carbon and sulfur in individual particles was mapped by energy-filtered transmission electron microscopy (EFTEM). Almost all particles analyzed contained a mixture of carbonaceous and sulfurous matter. Particles with satellites were found by EFTEM to contain both carbon and sulfur in the central particle, whereas in the satellite particles only carbonaceous material was detected.

Citation: Nguyen, H. N., et al. (2008), Chemical composition and morphology of individual aerosol particles from a CARIBIC flight at 10 km altitude between 50°N and 30°S, *J. Geophys. Res.*, *113*, D23209, doi:10.1029/2008JD009956.

1. Introduction

[2] Atmospheric aerosol particles have direct and indirect effects on Earth's climate. The most recent estimates of radiative forcing identify aerosol effects as bearing the largest uncertainties, in particular through their indirect effects on the properties of clouds [*Intergovernmental Panel on Climate Change*, 2007]. Moreover, the chemical characteristics of aerosol at higher altitudes are far less well studied than those of boundary layer aerosol. Nevertheless, the direct radiative forcing of organic aerosol in the lower free troposphere (2–6 km altitude) was estimated to be -0.26 W/m^2 [*Heald et al.*, 2006]. Although this pertained to a limited experimental area, the magnitude of this number is noteworthy. In the meantime, there is steady progress in aerosol research of which the aspects most relevant to our work are discussed below.

[3] Up to recently, general circulation models almost exclusively dealt with the sulfate aerosol constituent [*Rasch et al.*, 2000]. Studies using transmission electron microscopy (TEM) and energy-dispersive X-ray analysis (EDS) for elements with atomic number larger than ten on particles in the middle troposphere have found sulfurous aerosol to be dominant [*Okada et al.*, 2007]. During ACE-Asia, the carbonaceous fraction of the aerosol in the lower to middle part of the free troposphere was found to be considerably larger than the sulfurous fraction [*Huebert et al.* 2004; *Mader et al.*, 2002; *Maria et al.*, 2003]. The high concen-

[1]Division of Nuclear Physics, Lund University, Lund, Sweden.
[2]Division of Polymer and Materials Chemistry/nCHREM, Lund University, Lund, Sweden.
[3]Now at Center for Electron Nanoscopy, Technical University of Denmark, Kongens Lyngby, Denmark.
[4]Department of Electron Microscopy at the Medical Faculty, Lund University, Lund, Sweden.
[5]Fachgebiet Umweltmineralogie, Institut für Angewandte Geowissenschaften, Technische Universität Darmstadt, Darmstadt, Germany.
[6]Division of Atmospheric Chemistry, Max Planck Institute for Chemistry, Mainz, Germany.
[7]Leibniz Institute for Tropospheric Research, Leipzig, Germany.
[8]Atmospheric Composition Research, Royal Netherlands Meteorological Institute, De Bilt, Netherlands.
[9]Institute of Meteorology and Climate Research, Forschungszentrum Karlsruhe, Karlsruhe, Germany.

0148-0227/08/2008JD009956$09.00

trations of organic material could not be explained by chemical transport modeling [*Heald et al.*, 2005]. *Henze and Seinfeld* [2006] presented modeling results pointing at oxidation products of isoprene as a potentially strong source of free tropospheric aerosol. In a study over eastern North America, a strong decrease of the sulfate concentration with altitude, up to the ceiling of the measurement aircraft of 6 km, was observed. This was accompanied by weaker decrease of water-soluble organic compounds [*Heald et al.*, 2006; *Peltier et al.*, 2007], thus indicating growing relative importance of carbonaceous over sulfurous aerosol with altitude in the troposphere.

[4] In the upper troposphere (UT) and the lowermost stratosphere (LS), *Dibb et al.* [2000] measured the concentration of inorganic ions in the aerosol. Regularly undertaken measurements of elemental concentrations from the Civil Aircraft for Regular Investigation of the atmosphere Based on an Instrument Container (CARIBIC; http://www.caribic-atmospheric.com) platform have revealed the concentrations appearing in the upper troposphere [*Martinsson et al.*, 2001; *Papaspiropoulos et al.*, 2002]. The data have also been used to estimate the production of sulfurous aerosol in the stratosphere and the concentration in relation to air exchange across the tropopause [*Martinsson et al.*, 2005].

[5] Further insight has been obtained by single particle analyses using TEM and EDS. *Sheridan et al.* [1994] obtained upper tropospheric and lowermost stratospheric particle morphologies and X-ray-based elemental analyses that were interpreted as being predominantly sulfates. *Xu et al.* [2001] identified sulfuric acid as the dominating particle type of the UT/LS aerosol and *Kojima et al.* [2004] found that sulfate particles (including sulfuric acid) dominated all samples. In contrast, *Heintzenberg et al.* [1996] found a mode of one micrometer mineral particles that served as ice nucleation sites during a time period influenced by the volcanic eruption of Mt. Pinatubo. Additionally, *Petzold et al.* [1998] found that black carbon particles provided the dominant condensation sites (by number) to cirrus clouds and contrails studied. *Murphy et al.* [1998] pointed out that a large fraction of the upper tropospheric aerosol is carbonaceous, on the basis of single particle analysis by laser ablation and mass spectrometry. On the basis of relative intensities in mass spectra, the ratio of carbonaceous to sulfurous aerosol was estimated. Particles containing a carbonaceous/sulfurous mixture were found to be abundant in the upper troposphere, and their frequency of appearance was found to decrease with increasing altitude in the lowermost stratosphere [*Murphy et al.*, 2007]. Recently quantitative analyses of concentrations of light elements have been implemented in the CARIBIC aerosol analysis, showing that a major fraction of the upper tropospheric aerosol is carbonaceous [*Nguyen and Martinsson*, 2007].

[6] The strategy of our present study is to combine quantitative analysis and single particle analysis investigating the results in relation to meteorological and geographical data, and thus examining the variation of particle morphology and composition between the Northern and Southern hemispheres. Single particles analyses were obtained mainly by TEM and energy-filtered TEM (EFTEM), providing morphological information and elemental mapping, respectively. EFTEM has previously been applied to atmospheric particles by *Pósfai et al.* [2003] and *Chen et al.* [2005]. The single particle analyses were complemented with quantitative analyses by particle-induced X-ray emission (PIXE) and particle elastic scattering analysis (PESA). Aerosol samples investigated here were collected during one CARIBIC flight in the upper troposphere and the lowermost stratosphere between Frankfurt, Germany and Santiago de Chile. The samples showed large variability in morphological appearance, and the chemical composition was complicated with both sulfurous and carbonaceous constituents present in all particles analyzed by EFTEM.

2. Materials and Methods

[7] The CARIBIC system is deployed on a monthly basis in an automated container-laboratory onboard a Lufthansa Airbus Type A340–600 that is equipped with a special inlet system for aerosol and trace gas measurement [*Brenninkmeijer et al.*, 2007]. Here we focus on detailed analyses of nine aerosol sampling events along a flight leg from Frankfurt, Germany to Santiago de Chile with an intermediate landing in Sao Paolo, Brazil on 30 and 31 August 2005 (see Figure 1).

[8] The CARIBIC multichannel aerosol sampler is based on the impaction technique [*Nguyen et al.*, 2006]. Two kinds of samples were collected simultaneously; one for single particle analysis by electron microscopic methods TEM and EFTEM [*Ortner*, 1999], the other for quantitative analysis using PESA in combination with PIXE techniques. The latter samples, which have been described in detail by *Nguyen and Martinsson* [2007], were collected on thin polyimide film (AP1™). Two samples for electron microscopy were collected in each sampling channel on thin carbon films supported by a copper TEM grid (600 mesh). Each sampling event thus produces a set of three samples, in total 27 samples for the nine events covered here. The diameter of each of the two impactor jets which were used to collect TEM samples was 0.15 mm. The total sampling flow rate of the two jets used for electron microscopic samples was 0.37 l min^{-1}. The upper size limit was 2.0 μm in diameter, defined by a cyclone separator placed upstream of the sampler.

[9] Figure 2 shows part of the impaction area on a TEM copper grid covered by a carbon foil. This image was taken by environmental scanning electron microscopy (ESEM) using an FEI Quanta 200 FEG ESEM instrument (FEI, Eindhoven, Netherlands). To reduce evaporation losses, the instrument was operated at a sample chamber pressure of 1 to 5 mbar and a low acceleration voltage of 3 kV was chosen. Experimental details of ESEM technique are given by *Ebert et al.* [2002], who used ESEM to study size (equivalent projected area diameter) and morphology of the aerosol particles. As can be seen, some parts of the sample area were lost owing to film breakage that can be caused by the impactor jet as well as in the fabrication or handling of the substrates. Although the films were broken in some places, analyses could be undertaken on the undamaged parts of the film. The analyses based on transmission of electrons are carried out at the 25 × 25 μm grid holes. The distribution of particles on the impaction area is not uniform. Larger particles occurred near and at the center of the impaction area (the bottom left corner in Figure 2). Fewer and smaller particles appeared in the periphery of the

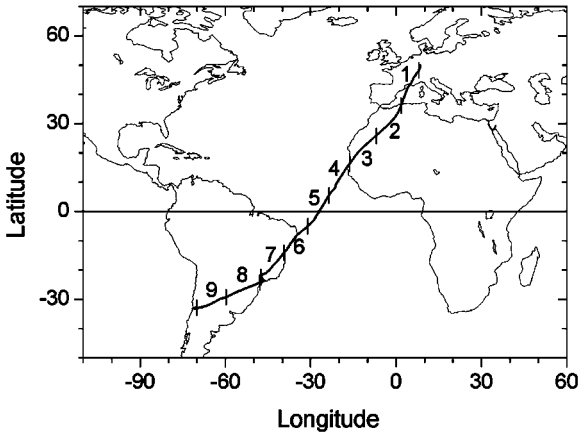

Figure 1. The CARIBIC flight track along which aerosol samples were collected. Numbers indicate the sampling positions, and the vertical bars indicate the limit between the different samples.

impaction area (the top right corner in Figure 2). The pattern observed here is typical for sampling by impaction.

[10] Many kinds of particles change their morphology upon collection on a surface, for instance an originally liquid, spherical sulfuric acid particle spreads out over a surface with a pattern of satellite particles surrounding a central part of the droplet. Large particles with high impaction velocity are preferentially collected in the impaction center. As a result, the particle deposit usually was dense in the central part, which can cause interactions between neighboring particles [*Wittmaack*, 2002]. We chose to present particles from the impaction center primarily because of they represent a large fraction of the aerosol mass. Identification of satellite patterns was not possible in the central part of the sample area. These patterns were mainly retrieved from the outer parts of the aerosol deposit. Despite the difference to the in situ morphology, analysis following collection of particles onto a surface is the established method for morphological analyses, and, at present the only way to obtain insights to the chemical distribution inside particles.

[11] TEM analysis of the aerosol samples was performed using a PHILIPS CM 10 transmission electron microscope operated at 100 keV. First, the center of the impaction area was located at low magnification (800X) and relatively low electron current density in order to reduce radiation damage to the sample. Next, the area from the center to the periphery of the impaction area was visualized by TEM images on photographic films (Kodak Electron Microscope Film 4489 (8.3 $\times$ 11.9 cm)) at higher magnifications (2200X) and with low electron current density. This area was a rectangle whose length was equal to the radius of the impaction area and its width was equal to the width of one square of the TEM grid. That way seven to eleven TEM images were taken for each sample. Thereby, an overview of the aerosol particles that were present in the sample could be obtained.

[12] Atomic force microscopy (AFM) [*Pósfai et al.*, 1998] was applied to obtain volumetric information on the particles, using a Dimension 3100 AFM (Veeco). The particle images were obtained using tapping mode AFM with a typical tapping rate of 0.8 Hz. The tip used was made of Si having a 12.5 nm radius.

[13] In the process of chemical analysis by electron microscopy the electron beam damages the aerosol particles. The degree of damage could be reduced by optimizing analysis area, electron dose and analysis time. However, the damages could not completely be avoided. The degree of the damage strongly depends on the analysis method applied. Initial tests using EDS (energy-dispersive detection of X-rays) induced severe damages to the particles in the samples. The most efficient local chemical analysis in the electron microscope utilizes electron detection rather than X-rays, because of low fluorescence yield of low-energy X-rays and the strongly forward-peaked electron beam compared with the isotropically emitted characteristic X-rays. EFTEM is based on electron detection and has the additional advantage that elemental mapping is obtained. Therefore this method was chosen to study chemical composition of the particles in this work. Despite the precautions taken, radiation damages were induced. Parts of the particles were sublimated or reorganized by the effects of the electron beam.

[14] The energy loss from interaction of an electron beam with the sample is used in EFTEM to produce elemental maps based on absorption edges at energies characteristic of the elements. The map is obtained as the result of an energy filtering technique, where electrons of well defined energy loss are selected for the production of an image of a part of the sample. Acquisition of EFTEM images was performed using a JEOL TEM-3000F microscope equipped with a Gatan Image Filter (GIF 2002). The microscope was operated at 300 kV using a convergence angle of less than 1 mrad and a 30 mrad collection angle. Electrons were detected using a YAG (yttrium aluminum garnet) scintillator and a CCD (charge-coupled device) camera. The elemental maps were obtained using a 3-window method, where two measurements were taken at electron energy loss slightly lower than the energy of the absorption edge of the

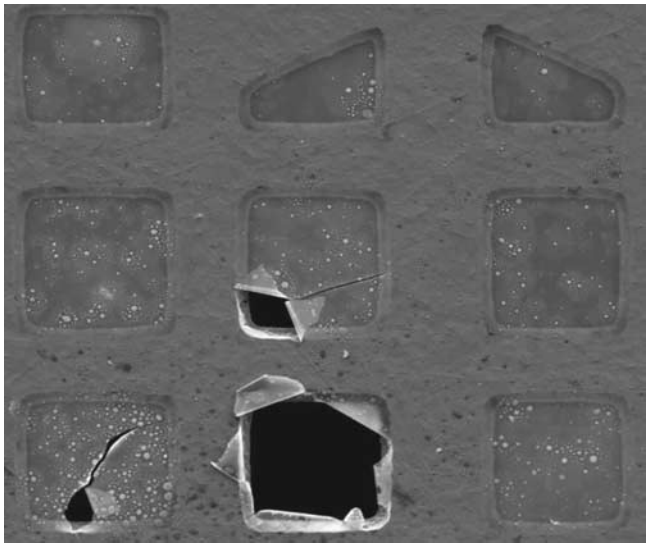

Figure 2. Picture of part of the impaction area using ESEM. The triangularly shaped holes mark the grid center, which normally does not coincide with the impaction center.

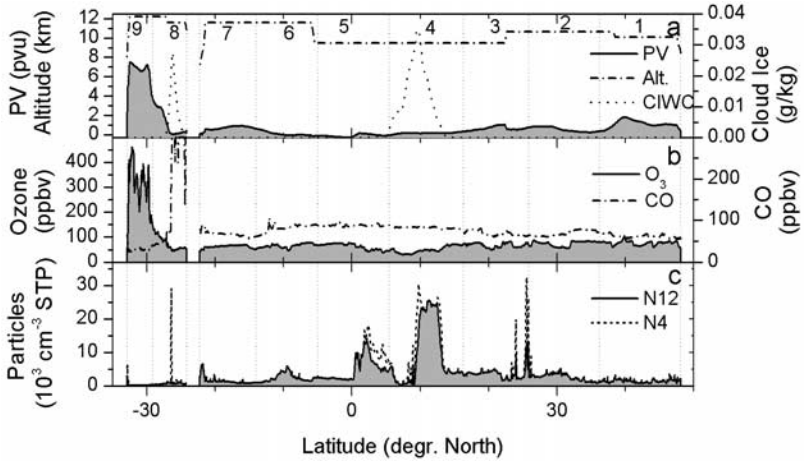

Figure 3. Parameters as a function of sampling latitude. The samples are numbered 1–9 in order of collection. (a) Pressure altitude (Alt.) of the flights and ECMWF analyses of cloud ice water content (CIWC) and potential vorticity (PV; 1 pvu = 10^{-6} m^2 s^{-1} K kg^{-1}), (b) trace gases ozone (O_3) and carbon monoxide (CO), and (c) number concentrations of particles with diameters larger than 4 nm (N4) and 12 nm (N12).

electronic level studied to estimate the background level and one at slightly higher energy loss. A thorough description of EFTEM applied to atmospheric aerosol particles is given by *Chen et al.* [2005]. In this study the magnification was 483000 times, producing imaged area of the dimensions 1.49 × 1.49 μm. Two elements were mapped by EFTEM. Carbon was analyzed by the K ionization edge at 284 eV and sulfur by the L ionization edge at 165 eV. An energy window of 20 eV was used for the pre and post edge data acquisition, each with duration of 20 s. The center energies were 130, 150 and 185 eV for sulfur and 252, 272 and 294 eV for carbon in the 3-window method. The carbon film thickness was 50 to 100 nm. The EFTEM limit of detection for carbon is estimated to be a 15 nm layer on this backing, and the detection limit of sulfur is estimated to be at a similar level. Images produced from EFTEM were background-subtracted using areas of each analyzed sample part that did not contain particles. This background subtraction technique was also used in an integration of the carbon and sulfur maps to obtain an estimate on their mass ratio in the analyzed part of the sample, based on ionization cross-sections, collection angle and energy window used.

[15] The nine samples that were collected for quantitative measurements were analyzed for elemental concentrations using PIXE and PESA to obtain the concentration of the major aerosol components present in each sample. These analytical methods have been described elsewhere [*Papaspiropoulos et al.*, 1999; *Nguyen and Martinsson*, 2007]. Here the results of the carbon and sulfur measurements were used. The minimum detection limits of these elements were 4 and 1.5 ng/m^3 STP (standard temperature pressure), respectively. The inaccuracy of the analyses is estimated to 10% [*Papaspiropoulos et al.*, 2002; *Nguyen and Martinsson*, 2007].

[16] Besides aerosol sampling for chemical analyses, CARIBIC instrumentation includes real time measurements of particle size distribution using three condensation particle counters (CPC). These instruments measure the integral

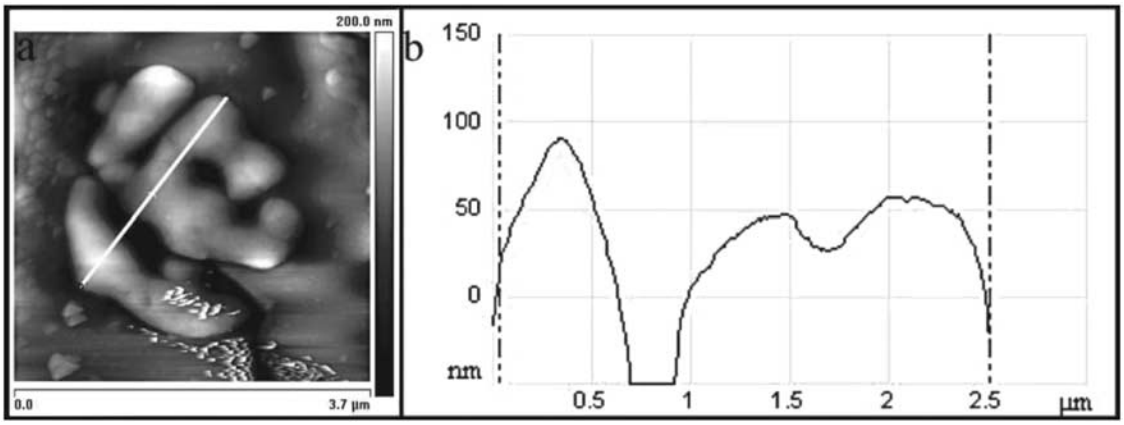

Figure 4. A particle at the center of the impaction area, imaged with AFM tapping mode. (a) Image giving the lateral dimensions and (b) cross section at the bright line in Figure 4a.

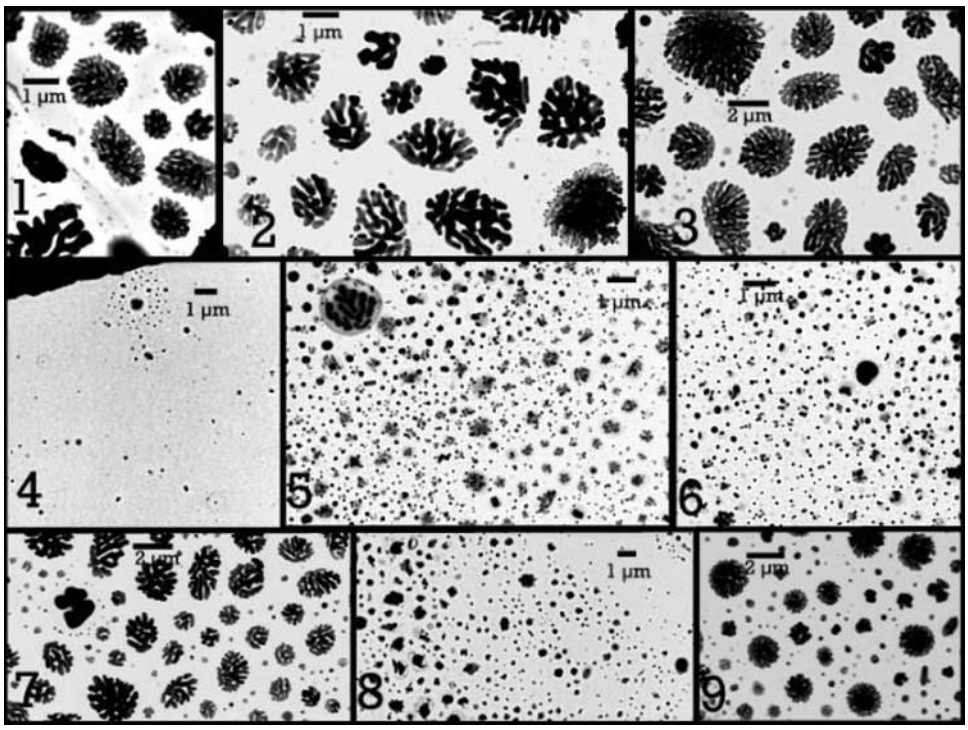

Figure 5. TEM images from the center of the impaction area of all nine samples.

particle number concentration of particles with sizes exceeding a selected threshold diameter. In this work data from two of the CPCs are used, i.e., number concentrations for particles larger than 4 nm (N4, indication of nucleation mode particles) and for particles larger 12 nm (N12, Aitken plus accumulation mode). The time resolution in the CPC measurements was set to 2 s and the inaccuracy is estimated to 10% [*Hermann et al.*, 2003; *Brenninkmeijer et al.*, 2007].

[17] Along with other trace gas species, O_3 and CO are routinely measured. Two systems are used for O_3 detection, namely an accurate, dual-beam UV-photometer and a fast solid-state chemiluminescence detector, where the former is used as the standard for the fast detector. The inaccuracy is estimated to 1% for 10 Hz measurements. CO measurements are obtained by a vacuum-UV instrument. The time resolution is 5 s and inaccuracy the larger value of 1.9% or 1 ppbv [*Brenninkmeijer et al.*, 2007].

[18] For CARIBIC data analysis, five-day backward trajectories were calculated to the position of the aircraft every third minute along the flight route. The computations were undertaken by the Royal Netherlands Meteorological Institute (KNMI) using the trajectory model TRAJKS [*Scheele et al.*, 1996], based on horizontal and vertical wind components from the European Centre for Medium-Range Weather Forecast (ECMWF). Potential vorticity (PV) and cloud ice water content (CIWC) were derived from archived ECMWF analyses with a resolution of 1×1 degree in the horizontal and 60 vertical hybrid sigma-pressure model levels. CIWC is a prognostic variable in the ECMWF model [*Tiedtke*, 1993], while PV is calculated from the temperature and wind fields. Both the PV and CIWC values were interpolated linearly in longitude, latitude, log pressure and time to the position of the aircraft.

3. Results and Discussion

[19] Sampling conditions were classified by the aid of the ECMWF-based modeling. The equator-ward outer limits of the sub-tropical jet streams according to the trajectory analysis were at 30°N and 12°S. These limits were used to define the extent of the tropics. The dynamical tropopause [*Hoerling et al.*, 1991; *Hoinka*, 1997] defined at 2.5 potential vorticity units (PVU) was used to discriminate between tropospheric and stratospheric air. From Figure 3a it can be seen that one of the samples, sample 9, was collected deep inside the lowermost stratosphere, with the average potential vorticity being 6.2 PVU. The stratospheric nature of the air mass is further confirmed by high ozone concentration (Figure 3b). Sample 8 was in part collected in the stratosphere. The part of that sample taken in the troposphere was affected by deep convection according to ECMWF analyses and the carbon monoxide concentration indicates that the up-transported air was polluted (Figures 3a and 3b). The remaining samples were taken in the upper troposphere. Out of these samples, numbers 1 and 7 were extratropical, numbers 3–6 tropical and number 2 was collected in both extratropical and tropical air. The intertropical convergence zone (ITCZ) was positioned at around 10°N according to ECMWF analyses. Ice cloud formation occurred reaching almost the 100 hPa atmospheric pressure level. In situ measurements and satellite imagery indicate that the clouds in the ITCZ are slightly further to the south, between 5.5 to 9.5°N, visible by the position of the local minimum in particle number (N4 and N12; Figure 3c) and

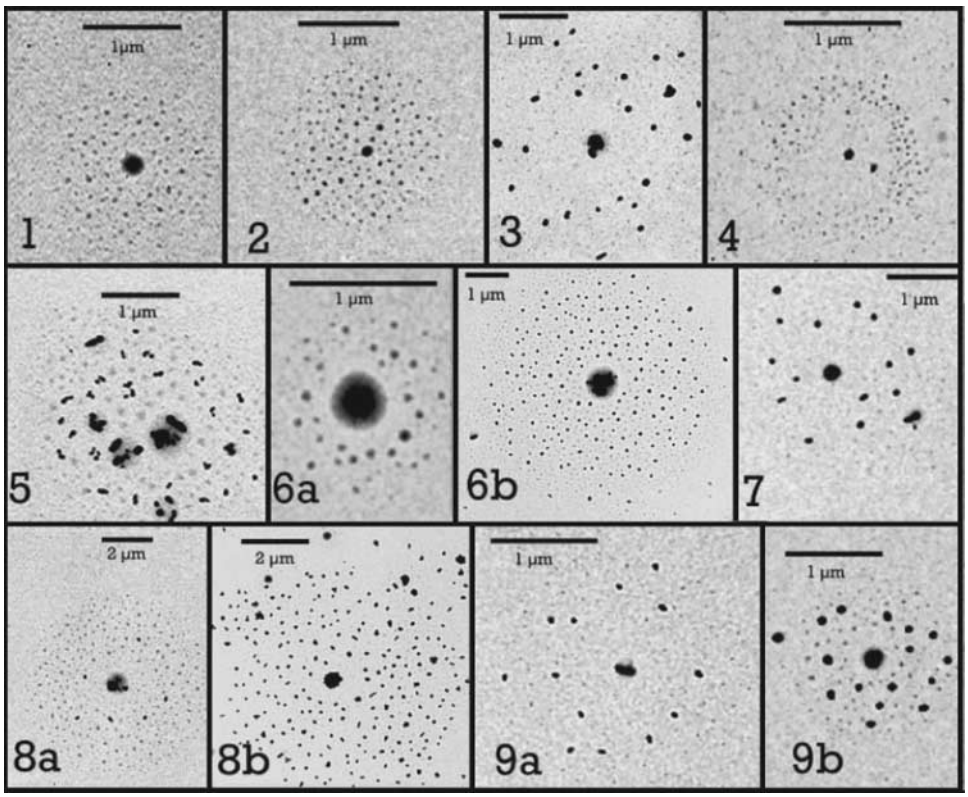

Figure 6. Frequently occurring particles with satellites selected from different parts (mostly on the periphery) of the impaction area from all nine samples.

ozone concentrations. Sample 4 was collected at the ITCZ and its outflow region. Carbon monoxide concentration showed no indication of polluted air being carried up by ITCZ clouds. The exchange of air across the ITCZ is small. Tropical samples 5 and 6 were taken to the south of ITCZ, whereas sample 3 is a representative of the northern tropics.

3.1. Particle Morphology

[20] TEM was used to investigate particle morphology. Some of the particles appeared to be large compared with the 2 μm diameter cutoff of the cyclone used to define the upper size limit of the sampling. In order to obtain information on the three-dimensional size of the particles, AFM was used. Figure 4 shows the AFM result for a particle from the center of the impaction area. This particle is an example for the kind of particle that showed large lateral dimensions (in, e.g., Figure 5, sample 2). It can be seen that even though the particle was about 2.5 μm in lateral extension, the height over the film extended less than 0.1 μm. These particles likely are not rigid, but change their shape as they are collected onto the film. Nevertheless, the particle volume-equivalent diameter was significantly smaller than the lateral extent according to the TEM analysis.

[21] Figures 5 and 6 give an overview of the particles in the samples. Figure 5 shows TEM images of the center of the impaction area from each of the nine samples. Interaction between neighboring particles might have affected the morphology in the relatively dense deposit of the impaction center. Generally, large particles appear in samples 1, 2, 3, 7 and 9. Small particles can be seen in samples 5, 6 and 8. The center of sample 4 in Figure 5 (labeled "4") contained only a small number of particles. This small number of particles collected is in sharp contrast to the high number concentrations registered by the CPCs (Figure 3c) in the outflow region of ITCZ. However, low concentration of large particles is one of the prerequisites favoring new particle formation. These particles most likely were too small to be collected by the impactor or too small to be detected by the low-dose and thus low-magnification technique used in the present TEM investigation.

[22] Figure 6 shows typical particles that were found on different parts (mostly on the periphery) of the impaction areas of all nine samples. All of them have satellite particles. The center particle of many particles is rounded (Figure 6, samples 1, 2, 4, 6a, 7, and 9b). Other center particles can be irregular in shape and/or comprise more than one component, where the latter is visible by the combined information from the shade of gray and the shape (Figure 6, samples 5, 6b, and 8a). The satellite patterns show large variability. The satellite particles can be rounded and in ordered pattern (Figure 6, samples 1, 2, and 6a) or irregular, rounded and rod-like particles in disordered pattern, including particles with less dark appearance in ordered pattern (Figure 6, sample 5). Many of the satellite patterns contain two or three distinct morphological components (Figure 6, samples 5, 6b, 8a, 8b, 9a, and 9b).

[23] The definitions of various particle types, their frequency of occurrence in each sample as well as illustrating images of the particle types are listed in Table 1. Particles were defined and classified into 10 groups (see the first column in Table 1). Among them, there are four main groups G (grains), O (irregular), R (rounded) and S

Table 1. Particle Types Observed in the Nine Samples Collected on Electron Microscope Grids

	Sample[a]										
	1	2	3	4	5	6	7	8	9	Number[b]	Figure[c]
Hemisp UT, LS region	NH UT extratrop	NH UT extratrop tropics	NH UT tropics	ITCZ UT tropics	SH UT tropics	SH UT tropics	SH UT extratrop	SH UT/LS extratrop	SH LS extratrop		
Particle type[d]											
G	-	-	-	-	C	c	-	-	-	2	5 (sample 5)
O	B	-	p	c,P	C	C	b,p	C,B,p	-	7	5 (samples 6 and 8)
Oi	-	-	B,P	-	B	-	P	B	b	5	6 (samples 3, 5, and 9a)
Ok	-	-	-	c	b,p	b,p	-	b,p	-	4	6 (samples 6b, 8a, and 8b)
R	-	b,p	-	b	b,p	B,P	c	P	p	7	5 (samples 4 and 7)
Ri	-	-	-	-	-	P	p	p	B,P	4	6 (samples 7 and 9b)
Rk	P	B,P	P	C,B	P	B,p	p	b	b,p	9	6 (samples 1, 2, 4, and 6a)
S	C	C	C	-	-	-	C	C	C,b	6	5 (samples 1–3 and 7–9)
V	c	-	-	-	-	-	B	c	-	3	5 (sample 8)
X	C,B	C,B	c,b	-	-	c,B	B	-	C,B	6	5 (samples 1–3 and 9)

[a]Position and frequency of the appearance of particle type in each sample. The positions are C (center of the sample), P (periphery of the sample) and B (between C and P). Large letter indicates large number fraction of particles (larger than 20%) and small letters small fraction, whereas hyphen indicates that the particle type was not found in the sample.

[b]Number of samples in which the particle type was found.

[c]Figure(s) where the particle type is shown.

[d]Particles/central particles: G, grains; O, irregular shape; R, rounded; S, complex and branching structure; V, rod-like; X, rounded, possibly satellite. Satellite patterns: i, irregular pattern; k, regular pattern.

(branched). Additional groups include infrequently appearing elongated (V) particles and rounded particles that could not be distinguished from satellites (X). For the main groups, satellite particles could often be seen clearly around particle types O and R, whereas type S particles mainly appeared in the dense deposit of the impaction center prohibiting identification of satellite patterns. The satellite patterns were classified in two groups regular (k) and irregular (i).

[24] Large particles are mostly found in the center of the impaction area, which is denoted C in Table 1. Many samples contained particle type S at the center of the impaction area. They were frequent in all extratropical samples and in the sample from the northern tropics (Figure 5, samples 1–3 and 7–9). The category does show some variation in morphology. In particular the type S particles from the stratospheric sample (Figure 5, sample 9) appear to be more compact than those from the tropospheric samples. The samples from southern tropics (Figure 5, samples 5 and 6) and the ITCZ (Figure 5, sample 4) contained very few type S particles. The particles are smaller, and in the case of the ITCZ sample significantly fewer. The most frequent particles in the latter sample are rounded with regular satellite pattern (Rk), whereas the largest particles in the southern tropics were of types O and G.

[25] Satellite patterns can be observed at the periphery (P) and in between (B) the center and the periphery of the impaction area. Both regular and irregular satellite patterns appear around O and R type central particles. From Table 1 it can be seen that a regular pattern is more connected with R particles and irregular patterns tend to be more common around O particles.

[26] The aerosol particle morphology varied a lot with the sampling location. This dependence is illustrated in Figure 5. The sample taken at the ITCZ (Figure 5, sample 4) contained fewer and smaller particles than the other samples. Many small particles as well as all the larger particles likely had been removed from the atmosphere by wet scavenging inside the tropical convective system. Thus, not many aerosol particles may have survived the "wet scrubbing" of the convective clouds. In the NH samples, many large particles (particle type S) could be seen (Figure 5, samples 1, 2, and 3) and in the extratropical SH sample as well (Figure 5, sample 7). They were presumably aged particles that were formed in the upper troposphere by different gas-to-particle conversion processes. As a result of their size, they dominate the mass concentration of these samples. Consequently, their chemical components dominated in these samples as well. In contrast, the tropical SH samples contain mostly smaller particles (Figure 5, samples 5 and 6), suggesting newly formed particles by gas-to-particle conversion processes.

3.2. Chemical Characterization

[27] The morphological study exposed several distinct features of the different particle types and some patterns connecting to sampling location, but the information is difficult to interpret. To further investigate the samples, chemical analyses were undertaken, where the morphological information served the purpose to guide in the selection of particles to be analyzed by EFTEM.

[28] In parallel to the sampling for electron microscopic analyses, samples were taken for ion beam analyses. PESA and PIXE were used to determine the elemental concentrations of carbon (C) and sulfur (S) of the samples. Figure 7 shows the S concentration and the concentration ratio C/S as a function of sampling latitude. The S concentration shows a clear minimum at 10°N, which was the sample taken at and close to the ITCZ, and in general, the concentration was lower in the tropics compared with extra-tropical latitudes. Several other elements besides sulfur can be detected by PIXE. Although sulfur always dominated among the elements detected with PIXE, occasionally concentrations in

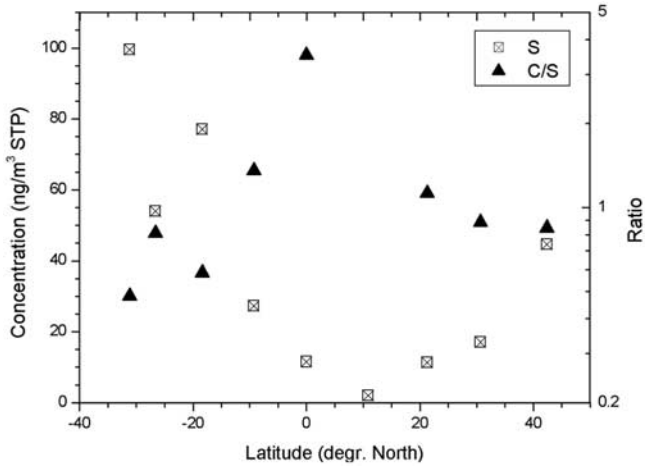

Figure 7. Concentration of sulfur (ng/m^3 STP) and the carbon-to-sulfur mass concentration ratio (C/S) in the nine samples. The concentration of carbon in sample 4 (at latitude 10°N) was lower than the detection limit, which, expressed in terms of C/S ratio, was 2.7 for this sample.

excess of 2% of the sulfur concentration appeared, most notably in the ITCZ sample where potassium, nickel and iron were present in concentration of 25, 10 and 7% by mass of that of sulfur. Sample 8 contained potassium corresponding to 3% of the sulfur concentration, possibly indicative of influence from biomass burning due to the coinciding high CO concentrations. Particularly high sulfur concentrations were found in the lowermost stratosphere (100 ng/m^3 STP) at latitude 31°S. The C/S mass ratio varied substantially over the samples in the range 0.5–3.5. The two highest values of the ratio appeared in the southern tropics in sample 6 and, in particular, sample 5. These samples stand out also with respect to morphology, by the absence of type S particles and the dominance of types O and G particles in the center of the impaction area (Figure 5). The lowermost stratospheric sample exhibited the lowest C/S ratio. Still, a substantial carbon fraction relative to sulfur was found in that sample. In order to investigate causes of the complex structures observed in the morphological analyses, EFTEM was used for identifying the distribution of carbonaceous and sulfurous matter within individual particles.

[29] EFTEM was applied to a selection of particle types identified in the morphology analysis. The EFTEM analyses resulted in images of the carbon and sulfur distributions in individual particles. Particles were selected for analysis from samples collected in different regions, namely extratropical samples from the NH (sample 1) and SH (sample 7), tropical samples from the NH, ITCZ and SH (samples 3, 4 and 5, respectively) and the lowermost stratosphere (sample 9). In each sample, the particles were chosen according to their frequency of occurrence. Results are presented in Figure 8. Figures 8a and 8b show images of the particles before and after the EFTEM analysis. Figure 8c shows red-green (RG) images which are a mixture of the carbon map (red) and the sulfur map (green) obtained from EFTEM analysis. Yellow and orange colors indicate mixture of the two elements.

[30] The images in Figure 8a often appear to contain more material than the ones in Figure 8b, indicating that these particles were partly sublimated by the electron beam during the EFTEM analysis or/and that the difference in electron energy (100 keV in Figure 8a and 300 keV in Figure 8b) causes differences in the contrast of the image. Although radiation damage is undesirable, a change of contrast clarifies sometimes underlying structures. For instance, the center particle in Figure 8a, particles 10 and 11, showed particles of irregular shape. Figure 8b, particles 10 and 11, indicates that they were actually agglomerates of smaller particles.

[31] Both Figures 7 and 8 contain information about carbon and sulfur concentrations that are obtained from different methodologies. In order to compare the results, the carbon and sulfur maps from EFTEM were integrated over the image area to obtain the ratio of the two elements. Noting that not all samples were selected for EFTEM analysis and that carbon could not be detected with PESA in sample 4, the results from EFTEM are related to PIXE-PESA in Figure 9. The EFTEM results were divided into three groups:

[32] 1. "Center, large particles": the largest particles appear in the center of the aerosol deposit (Figure 8, particles 1–5).

[33] 2. Periphery, large particles: From the periphery of the aerosol deposit (Figure 8, particles 10 and 11).

[34] 3. Periphery, small particles: From the periphery of the aerosol deposit (Figure 8, particles 6, 7, 9 and 12).

[35] Whereas the PIXE and PESA data are representative of the entire aerosol deposit, the EFTEM data are based on a small part of the sample that was selected from the morphological examination undertaken by TEM. The large particles in the center of the aerosol deposit carry most of the aerosol mass and compare fairly well with the PIXE-PESA results (Figure 9), although a deviation of more than a factor of 2 appears for one of the samples. The small particles from the periphery show a larger deviation, indicative of a larger carbon content of small particles. However, it should be borne in mind that only four examples are available from this study.

[36] The morphology of the large particles from the extratropics of the NH (Figure 5 (sample 1) and Figure 8a, particle 1) has a similar branched appearance as the large particles from the extratropics of the SH (Figure 5 (sample 7) and Figure 8a, particle 2). Between the branches, the shade of gray was similar to the background from the carbon film. A change of the contrast in the TEM image (not shown here) revealed that the area between the branches usually were darker than the background, thus indicating the presence of matter. The RG images (Figure 8c, particles 1 and 2) revealed the presence of carbonaceous matter between the branches, whereas the contrast of the TEM images mainly was caused by sulfurous matter inside the branches. Hence the particles are inhomogeneous in composition, consisting of both carbon- and sulfur-dominated parts.

[37] The morphology of the large particles from the tropics north of the ITCZ region and the ones from the tropics south of the ITCZ region is clearly different. This can be seen in Figure 5, samples 3 and 5. Both types of particles left C-rich and S-rich residues (see Figure 8c, particles 3 and 4). Especially, the sulfurous matter appeared

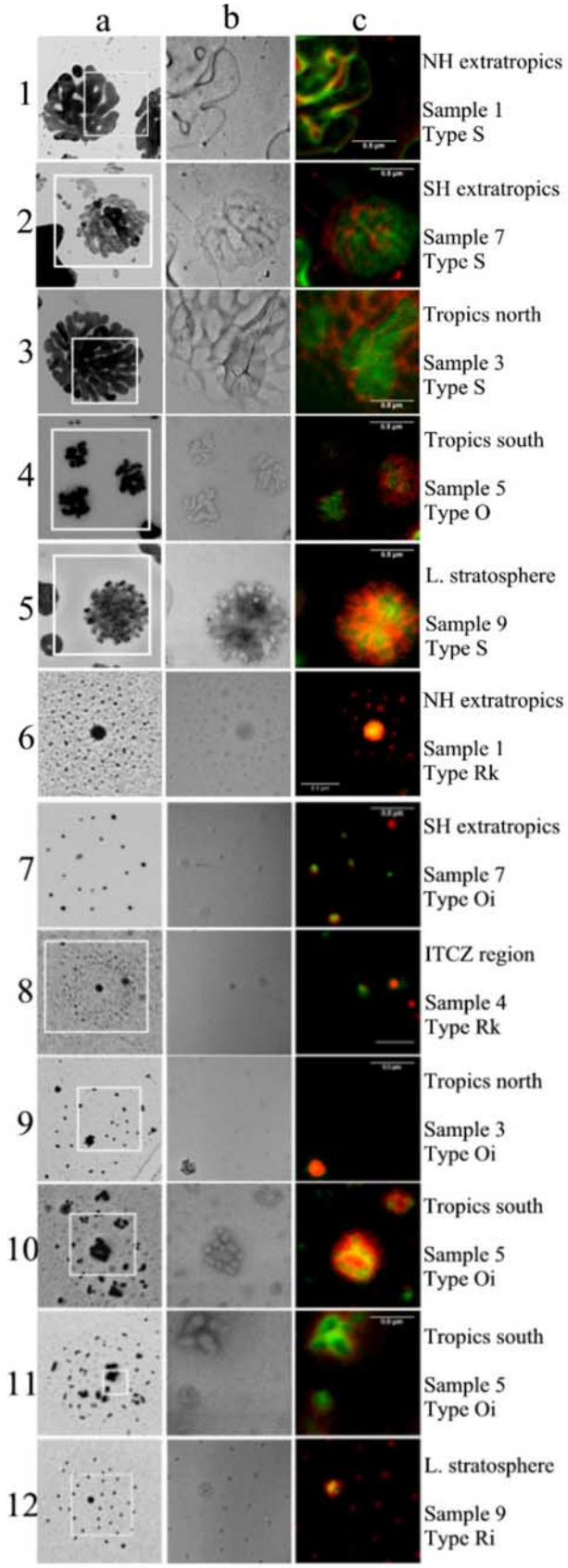

as inclusions in the carbonaceous part of the particle. However, a dislocation of the sulfur element can be seen in Figure 8c, particle 3. The sulfur element is believed to be surrounded by the carbon-rich material before the EFTEM analysis. During the EFTEM analysis, the energy input of the electron beam may have mobilized the sulfur by which it moved away from the branches to form a "pool" of sulfur-rich material, whereas the carbonaceous matter appears to be less affected by the electron beam (compare Figures 8a, 8b and 8c, particle 3). The NH tropics large particles show similar shape and elemental distribution as the large particles from the NH and SH extratropics. The large particles in the SH tropics differed markedly in morphology from large particles observed at other locations. Although these particles were damaged by the electron beam during EFTEM acquisition, the analysis shows that the residues of the particles contained both carbon and sulfur.

[38] The particle type in Figure 8a, particle 5, was common in the stratospheric sample. The center part of this particle shows a darker shade of gray and on the periphery of it a few small dark spots can be seen. In the TEM image taken after the EFTEM analysis, Figure 8b, particle 5, the center of the particle still is dark. However, the periphery shows bright spots. These bright spots indicate that the material in these parts was sublimated by the electron beam during the EFTEM analysis, indicating that material has been volatilized on the periphery of the particle. The RG image shows that the particle contains both carbon and sulfur. Carbon shows a spatial distribution similar to the TEM image whereas sulfur is localized mostly at the center part of the particle. This indicates that these lowermost stratospheric particles contrary to the upper tropospheric particles (Figure 8, particles 1–4) contain a "framework" of carbonaceous matter.

[39] The particles with satellite pattern in the NH extratropics contained both sulfur and carbon in their center (Figure 8c, particle 6). In the satellites, only carbon could be found. On the basis of the TEM image and the RG image, we interpret this particle type as being a droplet, possibly containing a solid core, the liquid being carbon-rich material. The particle shown in Figure 8a, particle 7 was not the same as the one that was analyzed with EFTEM (Figure 8b, particle 7, and Figure 8c, particle 7). However, they were of the same type according to the morphology-based classification. The center particle of this type could not be pointed out. The satellite particles varied in elemental composition. They contained both carbon and sulfur or only one of these elements.

Figure 8. Chemical distribution of individual particles. In Figure 8a, particles were imaged by the TEM technique in low magnification and at electron energy of 100 keV. Figure 8b shows the same particles or the same type of particles (images 6 and 7) but taken after EFTEM analysis (300 keV) and with higher magnification. Figure 8c shows EFTEM maps as mixed and colored images of sulfur (green) and carbon (red). Yellow and orange colors indicate mixture of the two elements. The text to the right shows sampling location, sample number, and particle type according to the classification of Table 1.

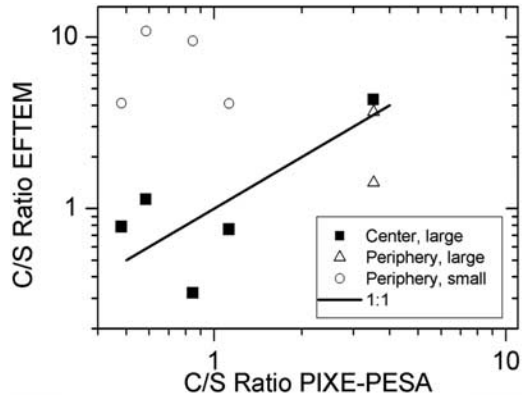

Figure 9. The carbon-to-sulfur ratio integrated from irradiated areas during EFTEM analysis according to Figure 8 related to that ratio obtained from the entire sample by PIXE and PESA. "Center, large" denotes large particles in the impaction center of the sample. "Periphery, large" and "Periphery, small" denote large and small particles at the periphery of the aerosol deposit.

[40] The particle from the ITCZ region in Figure 8, particle 8, contained a center particle and satellites which formed a band of particles around the center particle. The small satellites could not be seen in the S and C maps, because these satellite particles were too small to be imaged by the present EFTEM technique. Nevertheless, the center particle contained both sulfur and carbon.

[41] Comparing Figure 8b, particle 9, to Figure 8a, particle 9, reveals that almost all material in the satellites was sublimated by the electron beam. However, much material of the center particle still remained. Its morphology is similar to a soot aggregate consisting of many spherules. The result of the EFTEM analysis, image 9c, confirmed that they contained mostly carbon. Likely this soot particle had served as site for condensation of semi-volatile matter that was vaporized during the analysis. In the tropics south of the ITCZ, the center particle contained carbonaceous and sulfurous matter, and indications of agglomeration in the particle formation can be seen (Figure 8c, particles 10 and 11).

[42] A particle commonly found in the stratosphere with satellite pattern is shown in Figure 8, particle 12. The central particle contained both carbon and sulfur. The morphology according to the initial TEM image shows the presence of two kinds of satellites. The small satellites could not be detected in the EFTEM analysis, whereas the large ones were found to contain carbonaceous matter.

[43] A possible explanation of the morphology of the particle in Figure 8, particle 7, could be that this particle was an agglomerate particle before it impacted on the sampling substrate. The impaction may have caused this agglomerate chain to break. The primary particles of this agglomerate mostly had a sulfurous core coated with carbonaceous material. The agglomerates in Figure 8, particles 10 and 11, were also partly broken upon impaction. A closer examination of Figure 8b, particle 10, reveals that the agglomerated structure was partly preserved in the center of the particle where the carbonaceous matter clearly dominated over the sulfurous part according to EFTEM analysis. Possibly organic material acts as a binding substance, and the amount of organics might in this way affect the morphological identity of agglomerates after collection on the sample substrate.

[44] Particles with morphology exhibiting a center particle plus satellites such as the particle in Figure 8, particle 6, have been referred to in previous studies as sulfuric acid particles [*Bigg*, 1975, 1980; *Ferek et al.*, 1983; *Sheridan et al.*, 1994; *Xu et al.*, 2001; *Kojima et al.*, 2004]. However, the EFTEM analyses reveal that this particle type in our samples not only contained sulfur but also substantial amounts of carbon.

[45] In previous studies, the particle morphology according to Figure 8a, particles 1, 2 and 3, has often been classified as ammonium sulfate particles [*Buseck and Pósfai*, 1999; *Pósfai et al.*, 1999]. *Kojima et al.* [2005] suggested that these particles are coated with organic material. The EFTEM analyses of this work show that besides sulfur this particle type also contains substantial amounts of carbonaceous material.

[46] This study of individual particles reveals that upper tropospheric and lowermost stratospheric aerosol particles indeed are complicated both in terms of morphology and chemical composition. The concentrations of two elements were chosen to probe the composition and to represent sulfurous and carbonaceous aerosol constituents. Practically all particles analyzed contained both these elements in varying proportions. Morphological structures bear evidence of aerosol dynamical processes. The deep convective system probed in this study carried few particles that were small in size up to the altitudes studied here, in line with previous findings on particle scavenging of clouds with high updraft velocities [*Martinsson et al.*, 2000; *Schwarzenböck et al.*, 2000]. This indicates that the direct supply of particles from the boundary layer is small. High concentration of ultrafine particles indicative of recent new particle formation is frequently found in the outflow region of deep convective systems [*de Reus et al.*, 2001; *Heintzenberg et al.*, 2003; *Kanawade and Tripathi*, 2006; *Hermann et al.*, 2008], in particular under influence from solar radiation [*Hermann et al.*, 2003]. As evidenced by this new particle formation, aerosol precursor gases are present in connection with deep convections. Sulfurous and organic gases with low solubility partly escape in-cloud scavenging, thus forming reservoirs of trace gases that can take part in gas-to-particle formation at high altitude [*Kulmala et al.*, 2006]. The results of this study point to that the upper tropospheric submicrometer particulate mass to a large degree is being formed in situ from gaseous precursors. However, scavenging by clouds and precipitation is complicated, depending on cloud dynamical features as well as the pollution level of the air. The O_3 concentration was as low as 30 ppbv and the CO concentration did not show a local maximum during the ITCZ passage, indicating minor influence from combustion sources and pollution on the up-transported air [*Zahn et al.*, 2002]. The PIXE analyses do not reveal strong influences from pollution sources or other sources, since sulfur was the most abundant element even though clearly the lowest sulfur concentration during the entire transect from 50°N to 30°S. Taken together these conditions indicate that the observations were made under fairly unpolluted conditions. Increased pollution level has the tendency of decreasing the efficiency of scavenging in clouds, at least in early stages of cloud formation and development. Variability in cloud

dynamics need also to be considered before the indications of the present study of strong influence from in situ aerosol production in the upper troposphere can be generalized.

4. Conclusions

[47] Analyses of 27 aerosol samples representing nine sampling events in the upper troposphere and the lowermost stratosphere between Germany and Santiago de Chile, yielded detailed aerosol information that to a high degree reveals systematic patterns. Morphological examination based on transmission electron microscopy (TEM) identified different particle types. From these samples, a dependence of aerosol particle morphology on the sampling location was found. Large particles with branched structure were found in the NH (in the extra-tropics as well as the tropics) and in the extra-tropics of the SH. Particles in the ITCZ region were small and few, indicating that the removal mechanisms of the upward transport effectively precipitated all large particles and many of the small particles. Particles in the tropics of the SH were small in size but large in number concentration, suggesting their recent formation. The structure of large particles in the lowermost stratosphere was found to be more compact but still branched in a similar way as the large particles found in the extra-tropical upper troposphere. Particles with satellites appeared in all samples. The satellite pattern of the particles varied a lot, often with more than one kind of satellites surrounding the same particle.

[48] The quantitative analysis using PIXE (particle-induced X-ray emission) and PESA (particle elastic scattering analysis) showed that the mass concentration of particulate sulfur varied approximately by a factor of 50 over the nine samples analyzed here, where the lowest concentration appeared at the ITCZ and the highest in the lowermost stratosphere. The particulate carbon-to-sulfur concentration ratio by mass (C/S) varied between 0.5 and 3.5, with the lowest C/S ratio in the lowermost stratosphere and the highest in the tropics of the southern hemisphere.

[49] Analyses of individual particles with EFTEM (energy-filtered TEM) damaged the particles to varying degree. Nonetheless, the following results were obtained: (1) Almost all particles analyzed contained a mixture of carbonaceous and sulfurous matter. (2) Large particles showed complicated, branched structures where the sulfurous and carbonaceous fractions were spatially separated. (3) In particular the large stratospheric particles tended to be highly branched indicating carbonaceous interior surrounded by sulfurous matter. (4) Central particles of satellite-containing particles were chemically mixed. (5) Satellite particles were found to contain carbonaceous matter.

[50] The lowermost stratospheric particles differed from upper tropospheric ones by being more branched, which could possibly be connected with a difference in aerosol formation during the long residence time in the stratosphere. Particles with satellite patterns usually are interpreted as being composed of sulfuric acid. Analyses by EFTEM presented here show that these particles have a central particle composed of both carbonaceous and sulfurous matter whereas the satellites are composed of carbonaceous matter. Hence a morphological analysis alone could classify these mixed particles erroneously as being sulfuric acid.

[51] The results presented here indicate that small amounts of particulate matter were carried up to the upper troposphere by the tropical convective system. A possible explanation for the observed chemical and morphological patterns could be in situ production of particulate matter from pools of precursor gases, i.e., sulfur dioxide, dimethyl sulfide and organic gases. Photochemical transformations of gases transported from the boundary layer followed by aerosol dynamical processes of nucleation, condensation and coagulation is the likely cause of the complicated structures observed in the individual particle analyses.

[52] **Acknowledgments.** The collaboration with Lufthansa, providing an Airbus 340–600 adapted for the measurements, is gratefully acknowledged. Financial support for this work was provided by the Swedish Research Council for Environments, Agricultural Sciences and Spatial Planning under contract 214-2004-906. The support received from the European Science Foundation (ESF) for the activity entitled "Interdisciplinary Tropospheric Research: from the laboratory to global change" is gratefully acknowledged.

References

Bigg, E. K. (1975), Atmospheric particles, *J. Atmos. Sci.*, *32*, 910–917, doi:10.1175/1520-0469(1975)032<0910:SP>2.0.CO;2.

Bigg, E. K. (1980), Comparison of aerosol at four baseline atmospheric monitoring stations, *J. Appl. Meteorol.*, *19*, 521–533, doi:10.1175/1520-0450(1980)019<0521:COAAFB>2.0.CO;2.

Brenninkmeijer, C. A. M., et al. (2007), Civil aircraft for the regular investigation of the atmosphere based on an instrumented container: The new CARIBIC system, *Atmos. Chem. Phys.*, *7*, 4953–4976.

Buseck, P. R., and M. Pósfai (1999), Airborne minerals and related aerosol particles: Effects on climate and the environment, *Proc. Natl. Acad. Sci. U. S. A.*, *96*, 3372–3379, doi:10.1073/pnas.96.7.3372.

Chen, Y., N. Shah, F. E. Huggins, and G. P. Huffman (2005), Characterization of ambient airborne particles by energy-filtered transmission electron microscopy, *Aerosol Sci. Technol.*, *39*, 509–518, doi:10.1080/027868291001402.

de Reus, M., R. Krejci, J. Williams, H. Fischer, R. Scheele, and J. Ström (2001), Vertical and horizontal distributions of the aerosol number concentration and size distribution over the northern Indian Ocean, *J. Geophys. Res.*, *106*(D22), 28,629–28,641, doi:10.1029/2001JD900017.

Dibb, J. E., R. W. Talbot, and E. M. Scheuer (2000), Composition and distribution of aerosols over the North Atlantic during the subsonic assessment ozone and nitrogen oxide experiment (SONEX), *J. Geophys. Res.*, *105*, 3709–3717, doi:10.1029/1999JD900424.

Ebert, M., M. Inerle-Hof, and S. Weinbruch (2002), Environmental scanning electron microscopy as a new technique to determine the hygroscopic behaviour of individual aerosol particles, *Atmos. Environ.*, *36*, 5909–5916, doi:10.1016/S1352-2310(02)00774-4.

Ferek, R. J., A. L. Lazrus, and J. W. Winchester (1983), Electron microscopy of acidic aerosols collected over the Northeastern United States, *Atmos. Environ.*, *17*, 1545–1561, doi:10.1016/0004-6981(83)90308-6.

Heald, C. L., D. J. Jacob, R. J. Park, L. M. Russell, B. J. Huebert, J. H. Seinfeld, H. Liao, and R. J. Weber (2005), A large organic aerosol source in the free troposphere missing from current models, *Geophys. Res. Lett.*, *32*, L18809, doi:10.1029/2005GL023831.

Heald, C. L., et al. (2006), Concentrations and sources of organic carbon aerosols in the free troposphere over North America, *J. Geophys. Res.*, *111*, D23S47, doi:10.1029/2006JD007705.

Heintzenberg, J., K. Okada, and J. Ström (1996), On the composition of non-volatile material in upper tropospheric aerosols and cirrus crystals, *Atmos. Res.*, *41*, 81–88, doi:10.1016/0169-8095(95)00042-9.

Heintzenberg, J., M. Hermann, and D. Theiss (2003), Out of Africa: High aerosol concentrations in the upper troposphere over Africa, *Atmos. Chem. Phys.*, *3*, 1191–1198.

Henze, D. K., and J. H. Seinfeld (2006), Global secondary organic aerosol from isoprene oxidation, *Geophys. Res. Lett.*, *33*, L09812, doi:10.1029/2006GL025976.

Hermann, M., J. Heintzenberg, A. Wiedensohler, A. Zahn, G. Heinrich, and C. A. M. Brenninkmeijer (2003), Meridional distributions of aerosol particle number concentrations in the upper troposphere and lower stratosphere obtained by Civil Aircraft for Regular Investigation of the Atmosphere Based on an Instrument Container (CARIBIC) flights, *J. Geophys. Res.*, *108*(D3), 4114, doi:10.1029/2001JD001077.

Hermann, M., C. A. M. Brenninkmeijer, F. Slemr, J. Heintzenberg, B. G. Martinsson, H. Schlager, P. F. J. van Velthoven, A. Wiedensohler, A. Zahn,

and H. Ziereis (2008), Submicrometer aerosol particle size distributions in the upper troposphere over the north Atlantic—Results from the third CARIBIC route, *Tellus, Ser. B*, *60*, 106–117.

Hoerling, M. P., T. K. Schaack, and A. J. Lenzen (1991), Global objective tropopause analysis, *Mon. Weather Rev.*, *119*, 1816–1831, doi:10.1175/1520-0493(1991)119<1816:GOTA>2.0.CO;2.

Hoinka, K. P. (1997), The tropopause: Discovery, definition and demarcation, *Meteorol. Z. [Berlin]*, *6*, 281–303.

Huebert, B., T. Bertram, J. Kline, S. Howell, D. Eatough, and B. Blomquist (2004), Measurements of organic and elemental carbon in Asian outflow during ACE-Asia from the NSF/NCAR C-130, *J. Geophys. Res.*, *109*(D19), D19S11, doi:10.1029/2004JD004700.

Intergovernmental Panel on Climate Change (2007), *Climate Change 2007: The Physical Science Basis. Contribution of Working Group I to the Fourth Assessment Report of the Intergovernmental Panel on Climate Change*, edited by S. Solomon et al., Cambridge Univ. Press, Cambridge, U. K.

Kanawade, V., and S. N. Tripathi (2006), Evidence for the role of ion-induced particle formation during an atmospheric nucleation event observed in Tropospheric Ozone Production about Spring Equinox (TOPSE), *J. Geophys. Res.*, *111*, D02209, doi:10.1029/2005JD006366.

Kojima, T., P. R. Buseck, J. C. Wilson, J. M. Reeves, and M. J. Mahoney (2004), Aerosol particles from tropical convective systems: Cloud tops and cirrus anvils, *J. Geophys. Res.*, *109*, D12201, doi:10.1029/2003JD004504.

Kojima, T., P. R. Buseck, and J. M. Reeves (2005), Aerosol particles from tropical convective systems: 2. Cloud bases, *J. Geophys. Res.*, *110*, D09203, doi:10.1029/2004JD005173.

Kulmala, M., A. Reissel, M. Sipilä, B. Bonn, T. M. Ruuskanen, K. E. J. Lehtinen, V.-M. Kerminen, and J. Ström (2006), Deep convective clouds as aerosol production engines: Role of insoluble organics, *J. Geophys. Res.*, *111*, D17202, doi:10.1029/2005JD006963.

Mader, B. T., R. C. Flagan, and J. H. Seinfeld (2002), Airborne measurements of atmospheric carbonaceous aerosols during ACE-Asia, *J. Geophys. Res.*, *107*(D23), 4704, doi:10.1029/2002JD002221.

Maria, S. F., L. M. Russell, B. J. Turpin, R. J. Porcja, T. L. Campos, R. J. Weber, and B. J. Huebert (2003), Source signatures of carbon monoxide and organic functional groups in Asian Pacific Regional Aerosol Characterization Experiment (ACE-Asia) submicron aerosol types, *J. Geophys. Res.*, *108*(D23), 8637, doi:10.1029/2003JD003703.

Martinsson, B. G., et al. (2000), Validation of very high cloud droplet number concentrations in air masses transported thousands of kilometres over the ocean, *Tellus, Ser. B*, *52*, 801–814.

Martinsson, B. G., G. Papaspiropoulos, J. Heintzenberg, and M. Hermann (2001), Fine mode particulate sulphur in the tropopause region measured from intercontinental flights (CARIBIC), *Geophys. Res. Lett.*, *28*, 1175–1178, doi:10.1029/2000GL012257.

Martinsson, B. G., H. N. Nguyen, C. A. M. Brenninkmeijer, A. Zahn, J. Heintzenberg, M. Hermann, and P. J. F. van Velthoven (2005), Characteristics and origin of lowermost stratospheric aerosol at northern midlatitudes under volcanically quiescent conditions based on CARIBIC observations, *J. Geophys. Res.*, *110*, D12201, doi:10.1029/2004JD005644.

Murphy, D. M., D. S. Thomson, and M. J. Mahoney (1998), In situ measurements of organics, meteoritic material, mercury, and other elements in aerosols at 5 to 19 kilometers, *Science*, *282*(5394), 1664–1669, doi:10.1126/science.282.5394.1664.

Murphy, D. M., D. J. Cziczo, P. K. Hudson, and D. S. Thomson (2007), Carbonaceous material in aerosol particles in the lower stratosphere and tropopause region, *J. Geophys. Res.*, *112*, D04203, doi:10.1029/2006JD007297.

Nguyen, H. N., and B. G. Martinsson (2007), Analysis of C, N and O in aerosol collected on an organic backing using internal blank measurements and variable beam size, *Nucl. Instrum. Methods Phys. Res., Sect. B*, *264*, 96–109, doi:10.1016/j.nimb.2007.08.001.

Nguyen, H. N., A. Gudmundsson, and B. G. Martinsson (2006), Design and calibration of a multi-channel aerosol sampler for tropopause region studies from the CARIBIC platform, *Aerosol Sci. Technol.*, *40*, 649–655, doi:10.1080/02786820600767807.

Okada, K., M. Ikegami, Y. Zaizen, Y. Tsutsumi, Y. Makino, J. B. Jensen, and J. L. Gras (2007), Submicrometer sulfur-rich particles in the middle troposphere: Aircraft observations from Australia to Japan, *Atmos. Res.*, *88*, 185–198, doi:10.1016/j.atmosres.2007.10.012.

Ortner, H. M. (1999), Sampling and characterization of individual aerosol particles in occupational health studies, *J. Environ. Monit.*, *1*, 273–283.

Papaspiropoulos, G., B. Mentes, P. Kristiansson, and B. G. Martinsson (1999), A high sensitivity elemental analysis methodology for upper tropospheric aerosol, *Nucl. Instrum. Methods Phys. Res., Sect. B*, *150*, 356–362.

Papaspiropoulos, G., B. G. Martinsson, A. Zahn, C. A. M. Brenninkmeijer, M. Hermann, J. Heintzenberg, H. Fischer, and P. F. J. van Velthoven (2002), Aerosol elemental concentrations in the tropopause region from intercontinental flights with the Civil Aircraft for Regular Investigation of the Atmosphere Based on an Instrument Container (CARIBIC) platform, *J. Geophys. Res.*, *107*(D23), 4671, doi:10.1029/2002JD002344.

Peltier, R. E., A. P. Sullivan, R. J. Weber, C. A. Brock, A. G. Wollny, J. S. Holloway, J. A. de Gouw, and C. Warneke (2007), Fine aerosol bulk composition measured on WP-3D research aircraft in vicinity of the northeastern United States—Results from NEAQS, *Atmos. Chem. Phys.*, *7*, 3231–3247.

Petzold, A., J. Ström, S. Ohlsson, and F. P. Schröder (1998), Elemental composition and morphology of ice-crystal residual particles in cirrus clouds and contrails, *Atmos. Res.*, *49*, 21–34, doi:10.1016/S0169-8095(97)00083-5.

Pósfai, M., H. Xu, J. R. Anderson, and P. R. Buseck (1998), Wet and dry sizes of atmospheric aerosol particles: An AFM-TEM study, *Geophys. Res. Lett.*, *25*, 1907–1910, doi:10.1029/98GL01416.

Pósfai, M., J. R. Andersen, P. R. Buseck, and H. Sievering (1999), Soot and sulfate aerosol particles in the remote marine troposphere, *J. Geophys. Res.*, *104*, 21,685–21,693, doi:10.1029/1999JD900208.

Pósfai, M., R. Simonics, J. Li, P. V. Hobbs, and P. R. Buseck (2003), Individual aerosol particles from biomass burning in southern Africa: 1. Compositions and size distributions of carbonaceous particles, *J. Geophys. Res.*, *108*(D13), 8483, doi:10.1029/2002JD002291.

Rasch, P. J., et al. (2000), A comparison of scavenging and deposition processes in global models: Results from the WCRP Cambridge workshop 1995, *Tellus, Ser. B*, *52B*, 1025–1056.

Scheele, M., P. Siegmund, and P. van Velthoven (1996), Sensitivity of trajectories to data resolution and its dependence on the starting point: In or outside a tropopause fold, *Meteorol. Appl.*, *3*, 267–273.

Schwarzenböck, A., J. Heintzenberg, and S. Mertes (2000), Incorporation of aerosol particles between 25 and 850 nm into cloud elements: Measurements with a new complementary sampling system, *Atmos. Res.*, *52*, 241–260, doi:10.1016/S0169-8095(99)00034-4.

Sheridan, P. J., C. A. Brock, and J. C. Wilson (1994), Aerosol particles in the upper troposphere and lower stratosphere: Elemental composition and morphology of individual particles in northern midlatitudes, *Geophys. Res. Lett.*, *21*, 2587–2590, doi:10.1029/94GL01387.

Tiedtke, M. (1993), Representation of clouds in large-scale models, *Mon. Weather Rev.*, *121*, 3040–3061, doi:10.1175/1520-0493(1993)121<3040:ROCILS>2.0.CO;2.

Wittmaack, K. (2002), Impact and growth phenomena observed with submicrometer atmospheric aerosol particles collected on polished silicon at low coverage, *Atmos. Environ.*, *36*, 3963–3971, doi:10.1016/S1352-2310(02)00290-X.

Xu, L., K. Okada, Y. Iwasaka, K. Hara, Y. Okuhara, Y. Tsutsumi, and G. Shi (2001), The composition of individual aerosol particle in the troposphere and stratosphere over Xianghe (39.45°N, 117.0°E), China, *Atmos. Environ.*, *35*, 3145–3153, doi:10.1016/S1352-2310(00)00532-X.

Zahn, A., C. A. M. Brenninkmeijer, W. A. H. Asman, P. J. Crutzen, G. Heinrich, H. Fischer, J. W. M. Cuijpers, and P. F. J. van Velthoven (2002), Budgets of O_3 and CO in the upper troposphere: CARIBIC passenger aircraft results 1997–2001, *J. Geophys. Res.*, *107*(D17), 4337, doi:10.1029/2001JD001529.

C. A. M. Brenninkmeijer and T. Schuck, Division of Atmospheric Chemistry, Max Planck Institute for Chemistry, P.O. Box 3060, D-55020 Mainz, Germany.

E. Carlemalm, Department of Clinical Sciences, Lund University, SE-22362 Lund, Sweden.

M. Ebert and S. Weinbruch, Fachgebiet Umweltmineralogie, Institut für Angewandte Geowissenschaften, Technische Universität Darmstadt, Schnittspahnstr. 9, D-64287 Darmstadt, Germany.

J. Heintzenberg and M. Hermann, Leibniz Institute for Tropospheric Research, Permoserstrasse 15, D-04318 Leipzig, Germany.

B. G. Martinsson and H. N. Nguyen, Div. Nuclear Physics, Lund University, P.O. Box 118, SE-22100 Lund, Sweden. (bengt.martinsson@nuclear.lu.se)

P. J. F. van Velthoven, Atmospheric Composition Research, Royal Netherlands Meteorological Institute, P.O. Box 201, 3730 AE De Bilt, Utrecht, Netherlands.

J. B. Wagner, Center for Electron Nanoscopy, Technical University of Denmark, Building 307, DK-2800 Kongens Lyngby, Denmark.

A. Zahn, Institute of Meteorology and Climate Research, Forschungszentrum Karlsruhe, P.O. Box 3640, D-76021 Karlsruhe, Germany.